Stochastic simulation of resist linewidth roughness and critical dimension uniformity for optical lithography

Stewart A. Robertson
John J. Biafore
Mark D. Smith
KLA-Tencor Corporation
PCID Division
8834 North Capital of Texas Highway
Austin, Texas 78759
E-mail: stewart.robertson@kla-tencor.com

Michael T. Reilly
Jerome Wandell
Dow Electronic Materials
455 Forest Street
Marlborough, Massachusetts 01752

Abstract. The physical processes that underpin a recently developed commercial stochastic resist model are introduced and the model details discussed. The model is calibrated to experimental data for a commercially available immersion chemically amplified photoresist using basic physical information about the resist and an iterative fitting procedure. This data comprises CD (critical dimension) and LWR (linewidth roughness) measurements through focus and exposure for three separate line-type features on varying pitches: dense, semidense, and isolated. A root mean square error (RMSE) of 2.0 nm is observed between the calibrated model and the experimental CD data. The ability of the calibrated model to predict experimentally observed CD uniformity distributions is tested for a variety of 1-D and 2-D patterns under fixed focus and exposure conditions. The subnanometer RMSE obtained between experiment and simulation suggests that the calibrated stochastic model has excellent predictive power for a variety of applications. [DOI: 10.1117/1.3517090]

Subject terms: critical dimension distribution; line edge roughness; linewidth roughness; stochastic simulation, resist.

Paper 10055SSPRR received Apr. 14, 2010; revised manuscript received Sep. 22, 2010; accepted for publication Oct. 4, 2010; published online Dec. 1, 2010.

1 Introduction

In 1975, Dill and his colleagues published their seminal work on modeling photolithography[1,2] through the use of the mathematical equations that describe the underlying physical processes, particularly those of the nonlinear photoresist response.[3,4] The complexity of lithography modeling has increased considerably over the intervening period,[5] adding more rigorous mathematical descriptions of the optical system performance, mask topography effects, and different resist chemistries to name but a few enhancements. Although the use of such models has enabled researchers and lithographic engineers to study and solve a wide variety of practical research and manufacturing lithographic problems,[6] the underlying methods have almost exclusively utilized the continuum approximation. In this deterministic approach, the distribution of light and the resist chemical components is described through the use of continuous mathematical functions. While this technique can obviously describe the average behavior of a lithographic process with great accuracy, it ignores that the light energy distribution is quantized by photons and that the resist chemical species are spatially discrete in the form of molecules.

Many of the limiting factors for state-of-the-art lithography, such as linewidth roughness (LWR), critical dimension uniformity (CDU), and contact hole circularity, directly arise from the quantized nature of the exposing radiation and the resist film, they cannot therefore be predicted using the standard continuum approximation approach.

Although the majority of lithography simulation literature has concentrated on the continuum approach, a number have reported on stochastic (or probabilistic) modeling approaches to lithography simulation, where the quantization effects are included.[6–12] However, until recently commercial lithography simulation has relied exclusively on deterministic methods. In this paper, we study a model developed by Biafore et al.[13–15] and implemented in the commercial simulation software PROLITH^{TM} X3.1 (KLA-Tencor Corp, Milpitas, California). This resist model allows for two exposure mechanisms: direct photolysis and indirect exposure, where the photon energy ionizes the resist matrix and energy is passed to the acid generators by electron scattering. As this paper is concerned with immersion ArF lithography, only direct photolysis is considered; the indirect method is required only for high-energy photon cases, typified by extreme ultraviolet (EUV) exposure.

2 Stochastic Model Fundamentals

The stochastic model utilized in PROLITH X3.1 for direct photolytic exposure employs a physics-based Monte Carlo approach. As the simulation progresses, the probability of certain physical events occurring is calculated, and random numbers are used to determine the outcome.

The model assumes a simple material comprising of a single PAG (photoacid generator) species, a single base-quencher species, and a single polymer. The PAG loading and quencher loading (mean number of molecules per unit volume) are inputs to the model. At the start of each simulation run, the number of PAG molecules and the number of quencher molecules is calculated using Poisson statistics. Each of these molecules is then randomly placed within the resist domain. The remainder of the resist volume is considered to be the polymer matrix with no spatial fluctuation

1932-5150/2010/$25.00 © 2010 SPIE

in the number of protecting groups, principally because the density of protecting groups is orders of magnitude higher than that of the PAG or quencher.[13] The optical properties of the resulting film are determined by assuming a linear Beer's law approximation for the absorbance. The total absorbance depends on the PAG concentration and the PAG molar absorbance; the quencher concentration and the quencher molar absorbance; and the absorbance of the polymer resin.

The number of absorbed photons in a given resist volume can also be determined using the Poisson approximation. In this case, the mean number of photons for each volume is determined using a standard continuum calculation for the irradiance in the resist film, determining the amount of absorbed energy, and then dividing the resulting absorbed energy by the energy of a single 193-nm-wavelength photon.[14] The probability that a given photon is absorbed by a PAG molecule rather than by another species in the resist is calculated by comparing the local PAG absorption to total resist absorption in the volume of interest.

Once it has been determined that a photon has been absorbed by a PAG, the molecule is in an electronically excited state. The probability that the excited PAG produces an acid is given by the PAG quantum efficiency (ϕ); the probability that the excited PAG decays back to the ground state is given by $1-\phi$. In our model, PAG molecules that do not generate an acid are put back into their original state and are available for further photon absorption events. On completion of the exposure process, the simulation domain contains discrete locations for all the generated photoacids and the initial quencher population.

During the PEB (post-exposure bake) process, reaction-diffusion neutralization is simulated in the volume of interest. Acid and quencher are allowed to diffuse according to their rate constants; neutralization of acid by quencher occurs; as the acid diffuses, it is allowed to locally deprotect the polymer according to standard first order kinetics.

After the PEB process has been completed, development takes place. The rate of resist removal is mapped to deprotection extent using conventional dissolution rate equations.[16] However, in accordance with critical ionization theory the average deprotection level on a polymer molecule is considered rather than the instantaneous deprotection level.

3 Experimental Details

The goal of this study is to calibrate a stochastic resist model against experimental data, and then test the model predictions against independent data. The experimental calibration data were generated using an ASML/1900i in combination with a TEL Lithius i^+ track on 300-mm wafers. Three duplicate wafers were prepared with a 130-nm coating of Dow EPIC 2013 resist. The resist was applied over an organic dual layer BARC comprising of 79-nm of Dow AR26N under 19-nm of Dow AR19. JSR TCX041 topcoat was applied to the wafer stack at a thickness of 90-nm. Exposure were made utilizing a numerical aperture of 1.35 and an annular shaped source (0.9 outer sigma/ 0.6 inner sigma). The source was polarized using a standard XY configuration. Both the resist softbake and the PEB were performed at 100°C for 60 seconds. The resist film was developed for 12 seconds in DOW CD-26.

Each wafer was exposed with an identical focus-exposure matrix. Critical dimension (CD) data are collected using an Hitachi CD SEM (scanning-electron microscope) for three separate structures: 50-nm lines on 100-nm pitch, 80-nm lines on 200-nm pitch, and 110-nm lines on 700-nm pitch. At each site, the SEM image is captured and LWR calculated offline using SUMMIT (EUV Technology, Martinez, California). The SEM images were reviewed and sites that fail due to bridging, missing features, etc. were removed from the metrology analysis. Average CDs are calculated for those points in the focus-exposure matrices, where a valid CD measurement is obtained on all three wafers. A corresponding average 3σ LWR value was measured for each CD. The LWR values were calculated over a 400-nm line length, considering each of the lines in the SEM field of view. This was five lines for the 100-nm pitch, three lines for the 200-nm pitch, and one line for the 700-nm pitch.

Obviously, some output variance is driven by systematic differences between input conditions when different trials are run (e.g., small hotplate temperature differences or focus differences between exposure chucks). As it is very difficult and time consuming to identify and characterize all the sources, a simple attempt was made to minimize as many obvious systematic errors as possible. The track flow was balanced and restricted to a single unit for each process step, and the stepper job was configured to restrict exposures to a single stage. This procedure was used both for the collection of the calibration data set and the validation CD distribution data.

4 Model Calibration

The known model input settings were fixed to their measured (optical parameters) or theoretical (component loadings from resist formulation) values. These parameters included the PAG loading, the quencher loading, the polymer optical parameters, and the absorbance of both the PAG and quencher species. The remaining unknown parameters were optimized using an iterative fitting routine that minimized the error between predicted and observed values for CD and LWR. The fitted parameters include PAG quantum efficiency, photoacid diffusivity rate, quencher diffusivity rate, acid/quencher neutralization rate, the deprotection rate and the development rate equation parameters.

The figure of merit minimized is the chi square, or the variance, of the global error between simulation and experiment for the three mask features of interest

$$\chi^2 = \frac{\sum_i [x_i - f(x_i)]^2}{v},$$

where x_i is the value of the i'th experimental data point, $f(x_i)$ is the value of the i'th simulated data point (i.e., calculated by PROLITH), and v is the degrees of freedom. The model accuracy can be evaluated by comparison of the root mean square of the error (RMSE) between the three experimental trials and three simulated trials. The data points used in the optimization comprised of all available CD and LWR measurements.

Figure 1 compares the average of three stochastic simulation runs against the experimental mean CD for the three mask features studied. Figure 2 compares 3σ LWR between

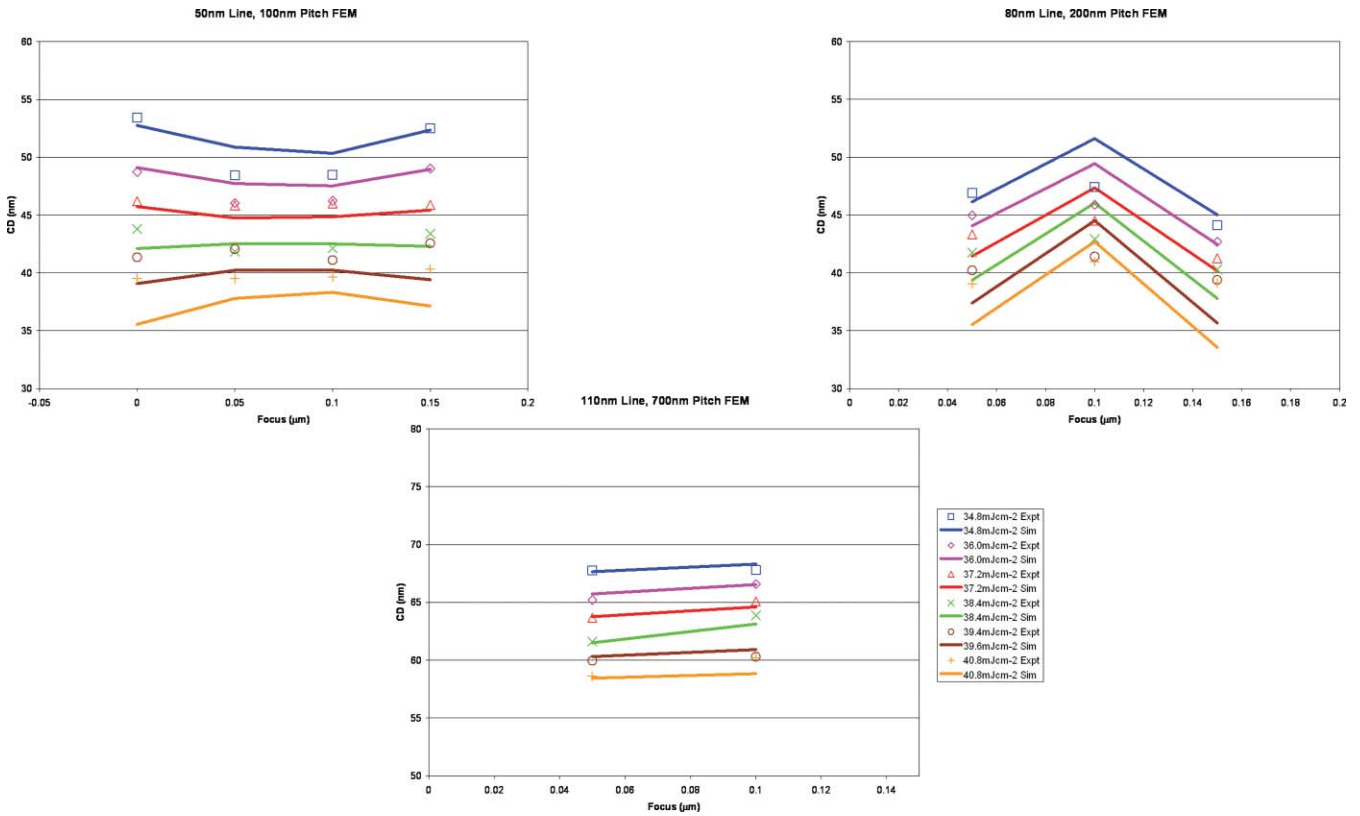

Fig. 1 Bossung plots comparing calibrated model versus experiment results. Plotted are simulated mean CD and experimental mean CD for three trials. Points are the experimental data; lines indicate simulation.

the three experimental trials and three simulated trials. For graphical clarity, the 3σ LWR values are averaged through dose at each focus value. The difference in LWR observed over the dose range was detectable but small, so this averaged approach does not skew the data excessively. For example, in the case of the 100-nm pitch line at a 0.05-μm focus, the experimental LWR results were 6.61, 5.82, 5.90, 5.56, 5.52, and 5.55 nm as the dose is increased from 34.8 to 40.8 mJ cm^{-2},

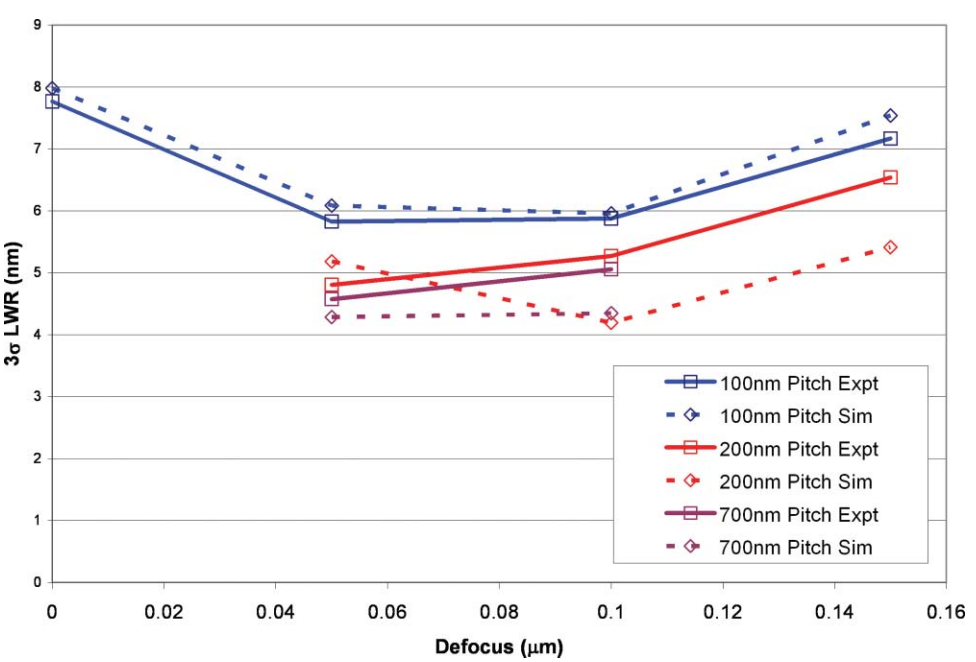

Fig. 2 Average 3σ LWR of three stochastic simulation trials against three experimental trials as a function of focus value, for all pitches.

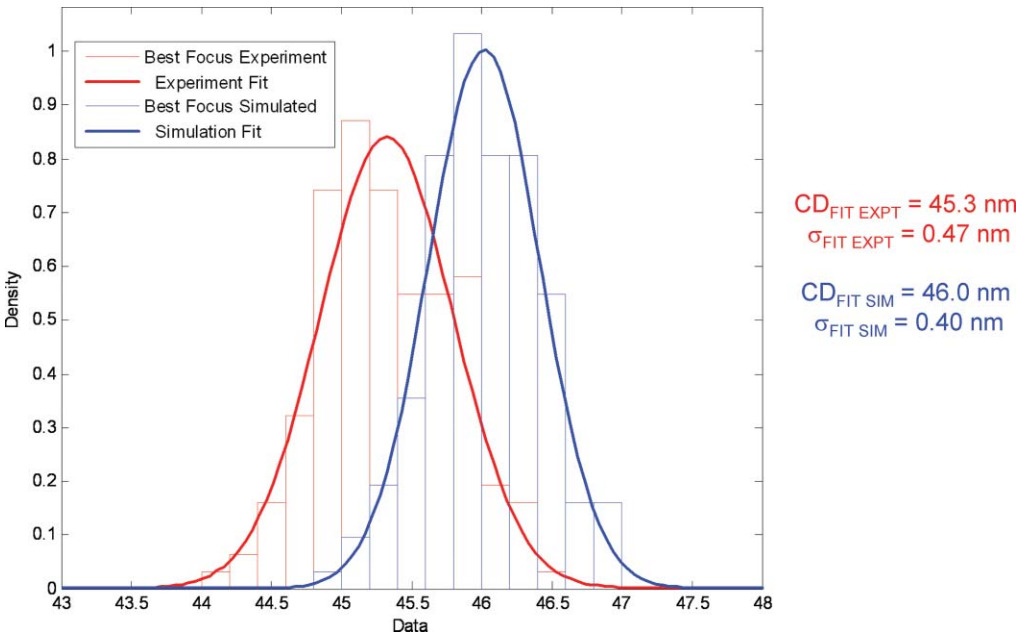

Fig. 3 Experimental and stochastic simulation of CD distribution for 50-nm lines on a 100-nm pitch at optimum exposure condition, 36.0 mJ cm $^{-2}$, 0.05-μm focus.

step 1.2 mJ cm^{-2} for and average LWR of 5.82 nm. The corresponding simulated LWR values were 6.64, 6.22, 6.56, 6.06, 5.65, and 5.36 nm for an average value of 6.08 nm. Both populations are quite tightly distributed around the mean value with a distinct decrease in LWR as the dose increases.

Table 1 summarizes the RMSE values for the calibrated parameter set. The simulated LWR values were determined over the same line length as the experimental data (400 nm), and the relevant number of lines were used for each pitch.

The optimized model parameter values appear consistent with physical expectations: the PAG quantum efficiency converged at around 15%, acid diffusivity was approximately 4 nm^2/s, quencher diffusivity was a little below 1 nm^2/s, while the developer contrast optimized at slightly under 20.

5 Predictions of CD Uniformity

Repeated stochastic simulation runs can be used to assemble simulated CDUs. The simulated CDU predictions can be compared to experiment for verification. In this paper, a large number of experimental CD measurements were produced. CDU data was collected for the 50-nm line on a 100-nm pitch (as used for calibration) and three different line-end shortening features. Each feature was measured 155 times comprising of 31 sites on five different wafers, the nominal focus and exposure dose for each site is identical.

Table 1 RMSE between experiment and stochastic simulation with optimized input parameters.

Feature	RMSE (CD)	RMSE (LWR)
50-nm line, 100-nm pitch	1.7 nm	1.0 nm
80-nm line, 200-nm pitch	2.8 nm	1.1 nm
110-nm line, 700-nm pitch	0.6 nm	0.8 nm
All	2.0 nm	1.0 nm

The first feature of interest was a 50-nm line in a 100-nm pitch imaged at 36.0 mJ cm^{-2} and 0.05 μm (best focus). The average CD for each point (simulated and experimental) was determined by considering the five lines in the SEM field of view over a 400-nm line length.

Figure 3 shows CDU plots for the experimental measurements and the stochastic simulation output for 155 separate trials. The simulation shows good agreement with experiment. The mean and standard deviation of the CD distributions for experiment and simulation are $\langle$CD expt.$\rangle$ = 45.3 nm, 0.47 nm 1 sigma, and $\langle$CD sim$\rangle$ = 46.0 nm, 0.40 1 sigma, respectively.

It is expected that the CD distribution should widen with defocus. This was tested by studying the same 50-nm line when the focus offset was increased by 0.1 μm. Figure 4 compares the experimental and simulated CDU. Again, good agreement between experiment and simulation is observed. We observe that mean CD for both experiment and simulation increases by 1.6 nm as a result of the focus shift. The standard deviations of the distributions increase to 0.55 and 0.56 nm for experiment and simulation.

The ability of the simulator to predict more complex 2-D patterns was also studied. The mask had a variety of line-end-shortening (LES) structures available. These consisted of gaps of varying length in the center line of a dense array of 50-nm lines in a 100-nm pitch. The gaps chosen for use were 100, 150, and 250 nm, the precise mask layouts are illustrated in Figs. 5, 6 and 7 respectively. The SEM metrology was chosen to return the minimum observed gap between the

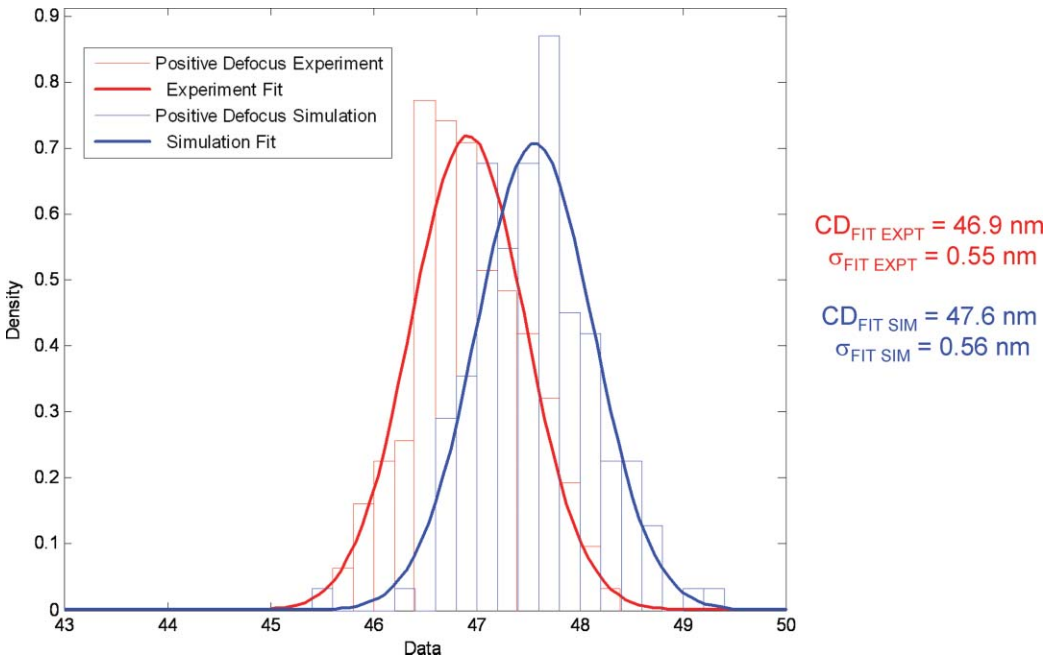

Fig. 4 Experimental and stochastic simulation of CD distribution for 50-nm lines on a 100-nm pitch at +0.10 μm above optimum focus, 36.0 mJ cm^{-2}, 0.15-μm focus.

line ends. The simulation metrology algorithm was set to mimic this behavior rather than return the gap size on a predetermined cut line.

Experimentally and within simulation, the printed gap length was measured for 155 sites for each case. The observed distributions with accompanying mean value and distribution statistics are detailed in Table 2 and Figs. 5 to 7. In all three cases, simulation predicts the experimental mean and variance of CD with good accuracy. The variance of CD distribution for the 2-D patterns is much larger than those for the linewidth measurements, and is observed in both experiment and simulation.

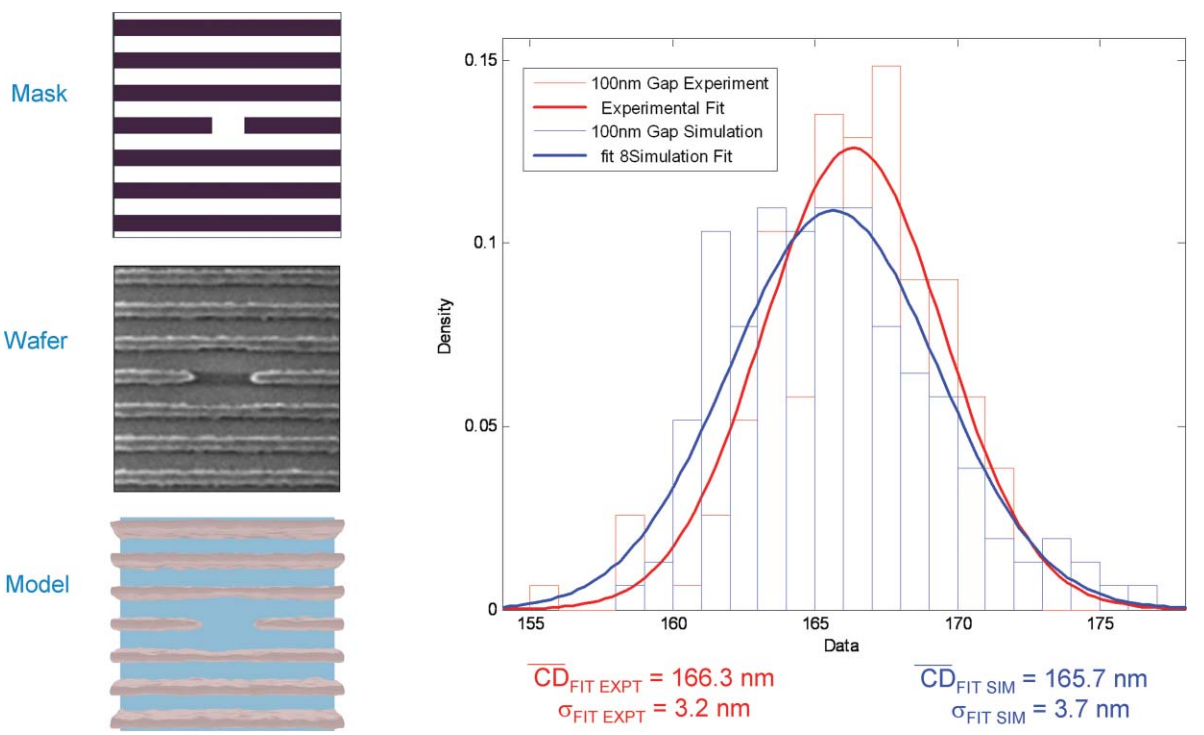

Fig. 5 Experimental and stochastic simulation of CD distribution for a 100-nm LES pattern at optimum exposure conditions, 36.0 mJ cm^{-2}, 0.05-μm focus. The mask layout and a representative SEM and stochastic resist simulation are shown for reference.

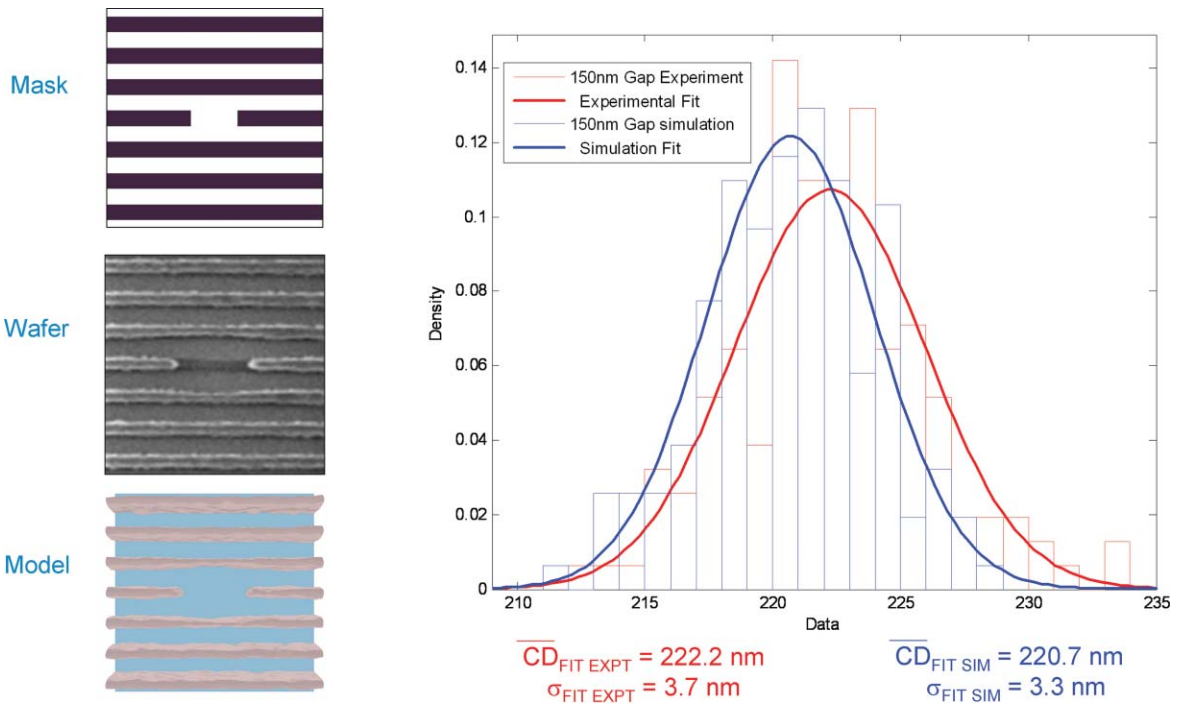

Fig. 6 Experimental and stochastic simulation of CD distribution for a 150-nm LES pattern at optimum exposure conditions, 36.0 mJ cm^{-2}, 0.05-μm focus. The mask layout and a representative SEM and stochastic resist simulation are shown for reference.

6 Conclusions

A new stochastic resist model was successfully calibrated to experimental results from a commercially available ArF immersion resist. When the resist model loading parameters and material optical parameters are constrained to their measured values, it would appear that the remaining kinetic parameters can be optimized effectively by considering mean CD and LWR values for focus-exposure matrices spanning a range of

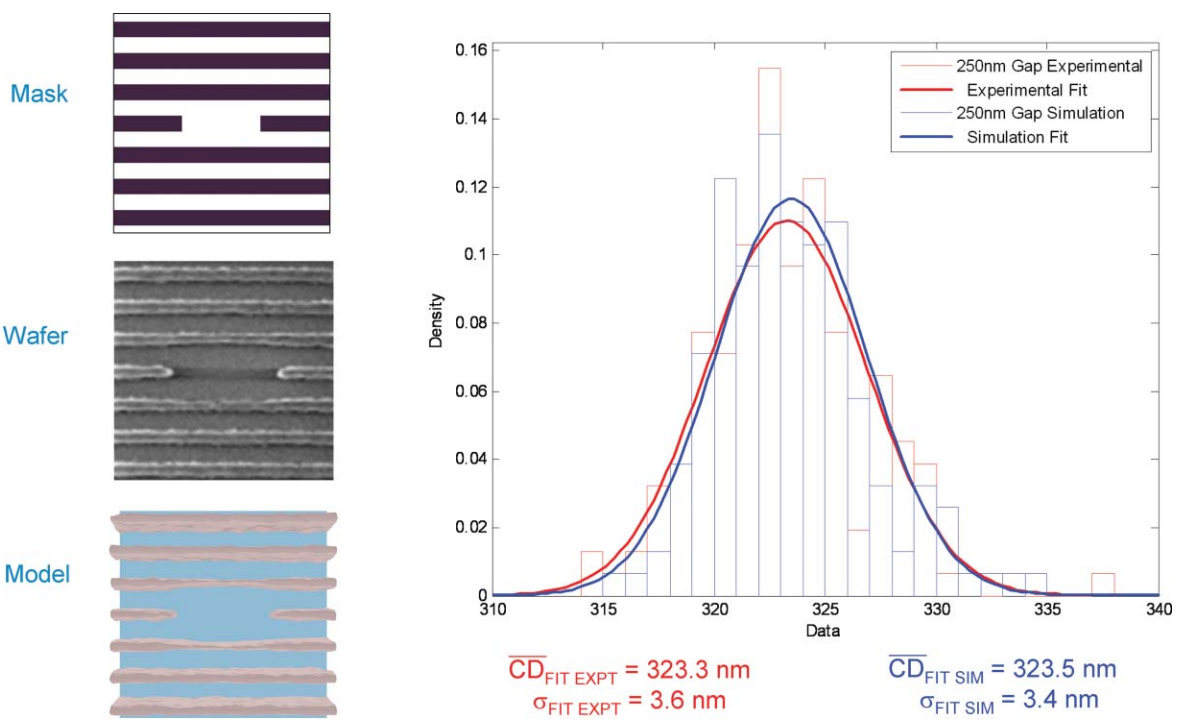

Fig. 7 Experimental and stochastic simulation of CD distribution for a 250-nm LES pattern at optimum exposure conditions, 36.0 mJ cm^{-2}, 0.05-μm focus. The mask layout and a representative SEM and stochastic resist simulation are shown for reference.

Table 2 Global model error, comparison of experimental mean and standard deviation of CD versus stochastic simulation.

Feature Type	Mean CD Experimental	Mean CD Simulation	Distribution σ Experimental	Distribution σ Simulation
50-nm line, 100-nm pitch, best focus	45.3 nm	46.0 nm	0.47 nm	0.40 nm
50-nm line, 100-nm pitch, positive defocus	46.9 nm	47.6 nm	0.55 nm	0.56 nm
100-nm gap LES	166.3 nm	165.7 nm	3.2 nm	3.7 nm
150-nm gap LES	222.2 nm	220.7 nm	3.7 nm	3.3 nm
250-nm gap LES	323.3 nm	323.5 nm	3.6 nm	3.4 nm
Average absolute deviation	0.74 nm		0.24 nm	

pitches. The resulting model was able to accurately predict CDU distributions for 1-D and more complex 2-D patterns with good accuracy.

Although our new model is straightforward, ignoring some intuitive sources of stochastic variation (such as polymer molecular weight polydispersity, varying protecting group content, and corresponding fluctuations in developer solubility), it describes the observed experimental behaviors well. Previous studies[13–15] comparing experimental data to simulation had suggested that the effects that are incorporated to the stochastic model dominated the LWR/CDU behavior, at least for the photoresist materials studied to date.

Further work on this model will include the exploration of the power-spectral content of the LWR predicted by the model and that property is affected by various process and material properties; such as PAG and quencher aggregation and mask linewidth variance.

Acknowledgments

The authors would like to thank and acknowledge the SEM metrology group at Dow Electronic Materials and the PROLITH development team at KLA-Tencor, particularly David Blankenship, Greg Floyd, and Chris Walker.

References

1. F. H. Dill, "Optical lithography," *IEEE Trans. Electron Dev.* **ED-22**(7), 440–444 (1975).
2. F. H. Dill, A. R. Neureuther, J. A. Tuttle, and E. J. Walker, "Modeling projection printing of positive photoresists," *IEEE Trans. Electron Dev.* **ED-22**(7), 456–464 (1975).
3. F. H. Dill, W. P. Hornberger, P. S. Hauge, and J. M. Shaw, "Characterization of positive photoresists," *IEEE Trans. Electron Dev.* **ED-22**(7), 445–452 (1975).
4. K. L. Konnerth and F. H. Dill, "In-situ measurement of dielectric thickness during etching or developing processes," *IEEE Trans. Electron Dev.* **ED-22**(7), 452–456 (1975).
5. C. A. Mack, "30 years of lithography simulation," in *Optical Microlithography XVIII, Proc. SPIE* **5754**, 1–12 (2005).
6. C. A. Mack, "Lithography simulation in semiconductor manufacturing," in *Advanced Microlithography Technologies, Proc. SPIE* **5645**, 63–83 (2005).
7. A. Saeki, T. Kozawa, S. Tagawa, H. B. Cao, H. Deng, and M. J. Leeson, "Monte Carlo simulation on line edge roughness after development in chemically amplified resist of post-optical lithography," in *Advances in Resist Materials and Processing Technology XXV, Proc. SPIE* **6923**, 69230S (2008).
8. T. Mulders, W. Henke, K Elian, C. Nolscher, and M Sebald, "New stochastic post-exposure bake simulation method," *J. Microlith. Microfab. Microsyst.* **4**, 043010 (2005).
9. A Philippou, T. Mulders, and E. Scholl, "Impact of photoresist composition and polymer chain length on line-edge roughness probed with a stochastic simulator," *J. Micro/nanolith. MEMS MOEMS* **6**, 043005 (2007).
10. M. D. Smith, "Mechanistic model of line-edge roughness," in *Advances in Resist Materials and Processing Technology XXIII, Proc. SPIE* **6153**, 61530X (2006).
11. G. Schmid, M. D. Stewart, S. D. Burns, and C. G. Willson, "Mesoscale Monte Carlo simulation of photoresist processing," *J. Electrochem. Soc.* **151**, G155–G161 (2004).
12. C. A. Mack, "Stochastic modeling of photoresist development in 2D and 3D," in *Advances in Resist Materials and Processing Technology XXVII, Proc. SPIE* **7639**, 76392L (2010).
13. J. J. Biafore, M. D. Smith, S. A. Robertson, and T. Graves, "Mechanistic simulation of line-edge roughness," in *Advances in Resist Materials and Processing Technology XXIV, Proc. SPIE* **6519**, 65190Y (2007).
14. J. J. Biafore, M. D. Smith, C. A. Mack, J. W. Thackeray, R. Gronheid, S. A. Robertson, T. Graves, and D. Blankenship, "Statistical simulation of resist at EUV and ArF," in *Advances in Resist Materials and Processing Technology XXVI, Proc. SPIE* **7273**, 727343 (2009).
15. J. J. Biafore, M. D. Smith, E. Van Setten, T. Wallow, P. Naulleau, D. Blankenship, S. A. Robertson, and Y. Deng, "Resist pattern prediction at EUV," in *Extreme Ultraviolet (EUV) Lithography, Proc. SPIE* **7636**, 76360R (2010).
16. C. A. Mack, "Development of positive photoresists", *J. Electrochem. Soc. Solid-State Sci. Technol.* **134**(1), 148–152 (1987).

Biographies and photographs of the authors are not available.